Membrane structure in isolated and intact myelins

H. Inouye, J. Karthigasan, and D. A. Kirschner
Department of Neurology Research, Children's Hospital, and Department of Neuropathology, Harvard Medical School, Boston, Massachusetts 02115

ABSTRACT The biochemical composition of myelin and the topology of its constituent lipids and proteins are typically studied using membranes that have been isolated from whole, intact tissue using procedures involving hypotonic shock and sucrose density gradient centrifugation. To what extent, however, are the structure and intermembrane interactions of isolated myelin similar to those of intact myelin? We have previously reported that intact and isolated myelins do not always show identical myelin periods, indicating a difference in membrane–membrane interactions. The present study addresses the possibility that this is due to altered membrane structure. Because x-ray scattering from isolated myelin sometimes consists of overlapping Bragg reflections or is continuous, we developed nonlinear least squares procedures for analyzing the total intensity distribution after film scaling, background subtraction, and Lorentz correction. We calculated electron density profiles of isolated myelin for comparison with membrane profiles from intact myelin. The change in the width of the extracellular space and the relative invariance of the cytoplasmic space as a function of pH and ionic strength that we previously found for intact nerve was largely paralleled by isolated myelin. There were two exceptions: isolated CNS myelin was resistant to swelling under all conditions, and isolated PNS myelin in hypotonic saline showed indefinite swelling at the extracellular apposition. However, electron density profiles of isolated myelins, calculated to 30 Å resolution, did not show any major change in structure compared with intact myelin that could account for the differences in interactions.

INTRODUCTION

The molecular organization of myelin membranes has been deduced from x-ray diffraction and biochemical analyses. Whereas intact tissue is used for the diffraction analysis, isolated myelin is used for the biochemical (including topological) studies. The isolated membranes are obtained from intact tissue of the peripheral or central nervous systems (PNS, CNS) after hypotonic shock and fractionation by sucrose gradient centrifugation (Norton and Poduslo, 1973). The purity of the membranes is typically assessed by their electron microscopic similarity to intact, multilamellar myelin. We have been using x-ray diffraction to determine to what extent the structure and interactions of the myelin membranes are preserved after isolation. We have previously shown that the period of myelin that was isolated from the PNS and CNS is similar to that of intact myelin under most conditions of pH and ionic strength; however, certain differences are apparent. In hypotonic media, isolated PNS myelin swells indefinitely (Karthigasan and Kirschner, 1988) whereas intact PNS myelin swells to a finite extent to arrays having periods 40–120 Å greater than the native ~180 Å-period (Inouye and Kirschner, 1988*a*). Under conditions of low ionic strength and alkaline pH, isolated CNS myelin retains a near-native period of ~155 Å (Sedzik et al., 1984; Karthigasan and Kirschner, 1988), whereas intact CNS myelin swells by ~70 Å from the native period (Inouye and Kirschner, 1988*a*). In the current study, we address the possibility that an alteration in molecular structure during the course of membrane isolation may account for these differences in swelling. To determine whether isolated myelin has the same membrane structure as intact myelin, we analyzed its x-ray diffraction patterns to ~30 Å spacing and calculated electron density profiles for the membranes. Previously, such profiles have been calculated only for myelin of intact tissue (Kirschner et al., 1984). Because isolated myelin often gives overlapping Bragg peaks or continuous intensity distributions, we developed procedures for treating the total x-ray scattering intensity. The analysis also provided estimates of the lattice distortion and of the variation in the cytoplasmic packing distance.

MATERIALS AND METHODS

Specimens

Myelin was isolated from whole sciatic nerve (PNS) and brain (CNS) of adult mice by discontinuous sucrose centrifugation (Norton and Poduslo, 1973). The purity of our preparations was assessed morphologically by electron microscopy and biochemically by lipid and protein analyses,

and enzyme assays as previously described (Karthigasan and Kirschner, 1988). Aliquots of the isolated myelin were incubated in media for 2–24 h at specified pH and ionic strength (Karthigasan and Kirschner, 1988). Whole sciatic and optic nerves were dissected from normal adult mice, and were treated similarly as the isolated myelin.

X-Ray diffraction

Diffraction experiments were carried out using nickel-filtered and double-mirror focused CuKα radiation from an Elliott GX-20 rotating anode generator (GEC Avionics, Hertfordshire, UK; 35 kV, 40 mA; 200 μm focal spot). The specimen to film distance was 171 mm. The diffraction patterns were recorded with direct exposure x-ray film (Eastman Kodak Co., Rochester, NY). Short exposures were usually recorded before the long exposures to monitor possible structural changes in the specimen during each long exposure. The spacings of the Bragg reflections were measured directly off the x-ray films viewed at 6× magnification, and the myelin periods were calculated according to Bragg's law. The films were digitized on a Photoscan P-1000 microdensitometer (Optronics International, Inc., Chelmsford, MA) using a 50-μm raster. The point-focused diffraction patterns were digitized using a computer program written by Josh Simons, Image Graphics Laboratory, Department of Neuroscience, Children's Hospital. The dimensions of the beam were recorded from three different experiments using the same camera geometry. Images of the beam were scanned in orthogonal directions on a 25-μm raster. The intensity profile of the direct beam was fit by a Gaussian. The integral widths were in the range of 266–292 μm for one direction and in the range of 323–366 μm for the other direction.

Measurement of the total intensity function *I(R)*

To adequately cover the wide intensity range of myelin diffraction, multiple films were used. The film factor α was determined from

$$\alpha = (1/M)\sum_{j=1}^{N} \cdot \left\{(1/m)\sum_{i=1}^{n}\sum_{k=1}^{n}[D_j(i) - D_0]/[D_j(i+k) - D_0]\right\}, \quad (1)$$

where $D_j(i)$ is the observed optical density at the jth position along scattering angle for the ith film after averaging the scattering at j and $-j$, D_0 is the fog density of the film (which is constant for different films) obtained from the average optical density (O.D.) behind the beam stop, n is the number of the film in the film stack, N is the number of optical density data points, m is the number of combinations for comparison between two sets of films satisfying the condition that both $D_j(i)$ and $D_j(i + k)$ are smaller than the linear range of the optical density on the film D(limit), and M is the number of points on the film satisfying the above condition. The top film was assigned $i = 1$. The total optical density I at the jth position was written as

$$I_j = (1/m_f)\sum_{i=1}^{n}[D_j(i) - D_0]\alpha^{i-1}, \quad (2)$$

where m_f is the number of the film satisfying the condition that $D_j(i)$ is smaller than D(limit).

A smooth polynomial function did not fit the background curve in the whole range of scattering angles, due mainly to the rapid intensity change near the beam stop and the gradual intensity change at wider angles. We therefore determined the background curve by a combination of two polynomials with order ≤ 5. The ranges of the background were chosen visually to obtain a smooth curve beneath the peaks. The observed total intensity $I_{obs}(R)$ was determined after background subtraction and applying the Lorentz-type correction factor $C(R)$, and normalized to give

$$\int_{R_1}^{R_2} I_{obs}(R)dR = 1 \quad (3)$$

in the range of the observed reciprocal coordinates from R_1 to R_2. For the powder-like diffraction pattern using a point-focused incident beam we used $C(R) = R^2$. The observed intensity was not smoothed.

When the Bragg reflections were so broad that the peaks overlapped, the whole curve was initially fit by peak functions (Gaussian, Cauchy, or Pearson VII; Young et al., 1980; Toraya et al., 1983) using a nonlinear least squares optimization routine (see below). For the peak fitting, the input parameters consisted of the measured positions, heights and half-widths of the peaks. The iteration was terminated when the goodness of fit was within 1% of that of the previous cycle. The integral intensities and widths of the reflections were obtained after separating the overlapped peaks. These values were used as the input values for the optimizations.

Calculation of the total intensity function

According to paracrystalline theory (Hosemann and Bagchi, 1962; Guinier, 1963; Schwartz et al., 1975) the total intensity function I_{calc} is

$$I_{calc}(R) = b(R) * \{N[\langle F^2(R)\rangle - \langle F(R)\rangle^2] + 1/d\,\langle F(R)\rangle^2[Z(R) * |\Sigma(R)|^2]\}. \quad (4)$$

The symbols $\langle\,\rangle$ and $*$ are the averaging and convolution operations, respectively. The first term corresponds to the diffuse scattering and the second term corresponds to the Bragg reflections. $Z(R)$ is the interference function, $|\Sigma(R)|^2$ arises from the Fourier transform of the step-function expression for the extent of the lattice, $F(R)$ is the Fourier transform of a pair of membranes, N is the number of lattice points, d is the myelin period, and $b(R)$ is the shape function fit to the direct beam. The diffuse intensity arises from the cytoplasmic packing variation β (which is taken as the standard deviation of the Gaussian function) around the average cytoplasmic packing distance $2u$ (Schwartz et al., 1985). The interference function $Z(R)$ is written as

$$Z(R) = [1 - H^2(R)]/[1 + H^2(R) - 2|H(R)|\cos(2\pi dR)], \quad (5)$$

where $H(R) = \exp(-2\pi^2R^2\Delta^2)$. $H(r)$ is the Fourier transform of the Gaussian probability $h(r)$ having a standard deviation Δ, where $h(r)$ is the distribution function for nearest neighbors.

The $|\Sigma(R)|^2$ is written as

$$|\Sigma(R)|^2 = (Nd)^2\sin^2(\pi RNd)/(\pi RNd)^2. \quad (6)$$

Because the diffuse intensity and the structure amplitude change gradually the integral width of the Bragg reflection w is described as

$$w^2 = b^2 + (1/Nd)^2 + (\pi^4h^4/d^2)(\Delta/d)^4, \quad (7)$$

where b is the integral width of the Gaussian form of the direct beam and h refers to the hth order reflection. The second and third terms are integral widths of $|\Sigma(R)|^2$ and $Z(R)$, respectively. The first approximate

values of N and Δ were obtained from the plot of w^2 as a function of h^4 (Inouye and Kirschner, 1984; Alexander, 1969).

When there is no interference between membrane pairs (i.e., $Z(R) = 1$ within the range of observed R) the second term of Eq. 4 becomes $N\langle F(R)\rangle^2$ because $\int|\Sigma(R)|^2 = Nd$. Given $N = 1$, the total intensity function $I_{calc}(R)$ is described as

$$\begin{aligned} I_{calc}(R) &= b(R)^*\langle F^2(R)\rangle \\ &= b(R)^*\{2[A^2(R) + B^2(R)] \\ &\quad + 2G(R)[(A^2(R) - B^2(R)]\cos(4\pi uR) \\ &\quad - 2A(R)B(R)\sin(4\pi uR)]\} \end{aligned} \quad (8)$$

where $b(R)$ is shape of the direct beam, $A(R)$ and $B(R)$ are the symmetric and asymmetric parts of the Fourier transform of the asymmetric unit of a pair of membranes (with origin ar $r = \pm u$), and $G(R)$ is the Fourier transform of the Gaussian probability with standard deviation β. Eq. 8 corresponds to Eq. 36 of Schwartz et al. (1975). An identical equation may be derived for a pair of membranes whose separation is described by a Gaussian distribution (Pape et al., 1977; Nelander and Blaurock, 1978; Worthington, 1986, 1988).

Nonlinear least squares optimization

The value to be minimized is

$$\chi^2 = \Sigma\,[I_{obs}(R) - I_{calc}(R)]^2\,. \quad (9)$$

The difference between the new parameter value p_i from that of the initial value a_i for the ith parameter were obtained from the matrix product of A^{-1} and V where

$$\begin{aligned} &\mathbf{x} = \mathbf{A}^{-1}\,\mathbf{V}, \\ &x_i = p_i - a_i, \\ &A_{ij} = \Sigma\,\{[\partial I_{calc}(R, a_1, \ldots, a_n)/\partial p_i] \\ &\qquad \cdot [\partial I_{calc}(R, a_1, \ldots, a_n)/\partial p_j]\}, \text{ and} \\ &V_i = \Sigma\,\{I_{obs}(R) - I_{calc}(R, a_1, \ldots, a_n)\} \\ &\qquad \cdot \partial I_{calc}(R, a_1, \ldots, a_n)/\partial p_i. \end{aligned} \quad (10)$$

The uncertainty $\sigma(p_i)$ of the parameter p_i was obtained according to

$$\begin{aligned} &\sigma(p_i)^2 = \sigma^2\, e_{ii}, \text{ and} \\ &\sigma^2 = \Sigma\,[I_{obs}(R) - I_{calc}(R, p_1, \ldots, p_n)]^2/ \\ &\qquad \cdot (N - n - 1), \end{aligned} \quad (11)$$

where e_{ii} is the diagonal components of the A^{-1} (error matrix), N is the number of the observed data points, and $n + 1$ is the number of the parameters. We used Marquardt's algorithm (Bevington, 1969) to facilitate the convergence. The goodness of fit, or R-factor, is

$$R\text{-factor} = \Sigma\,|I_{obs} - I_{calc}|/\Sigma\,|I_{obs}|. \quad (12)$$

For the calculation of the partial derivatives of Eq. 10, we chose the increments to be 1% of the initial parameters. The iterative cycle of the least squares routine was terminated when the difference of the R-factor from its previous value became <1%. After achieving the initial convergence the increments were decreased 10-fold to optimize further for some x-ray patterns.

RESULTS

The objective of our previous structural study of isolated myelin was to determine to what extent intermembrane interactions are similar in isolated and intact myelins (Karthigasan and Kirschner, 1988). The assessment was based on a qualitative comparison of the x-ray diffraction patterns and measurement of the periods. Our finding of altered periods in isolated myelin prompted us to develop procedures for quantitating such patterns so that electron density profiles from isolated myelin could be compared with those from intact myelin.

Analysis of continuous scattering from isolated PNS myelin

Isolated myelin treated in hypotonic saline or distilled water showed two broad intensity maxima centered at ~80 Å and 40 Å spacings (Figs. 1 and 2 *A*). The heights and positions of the maxima and the depth of the minimum between them varied according to the treatment. As we previously suggested (Karthigasan and Kirschner, 1988), these maxima correspond to the maxima of the Fourier amplitude of a pair of membranes (Worthington and Blaurock, 1969; Caspar and Kirschner, 1971; Kirschner and Caspar, 1972). Our data differed from the calculated Fourier transform for a pair of membranes in showing elevated rather than zero intensity between the two maxima. This elevated intensity may be accounted

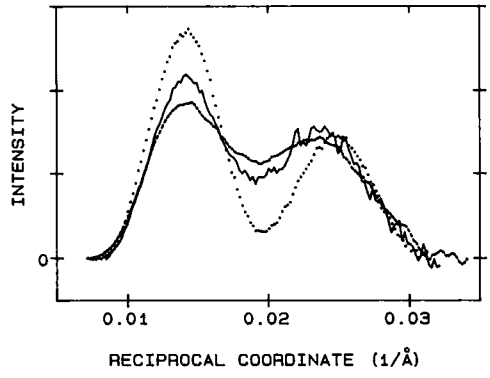

FIGURE 1 Densitometer tracings of x-ray diffraction patterns from isolated PNS myelin. Intensity distributions after background subtraction, Lorentz correction and normalization for samples treated at pH 7.4 and ionic strength 0.06 (*solid line*), pH 9.0 and ionic strength 0.06 (*dashed line*), and distilled water (*dotted line*). The diffracted intensity is continuous and does not show the discrete reflections that are typical of intact PNS myelin treated in a similar manner (see Fig. 2, *A* and *B*, and Fig. 2 *B* in Karthigasan and Kirschner, 1988). Note that the relative heights of the intensity maxima and the depth of the minimum between them depend on the incubation conditions.

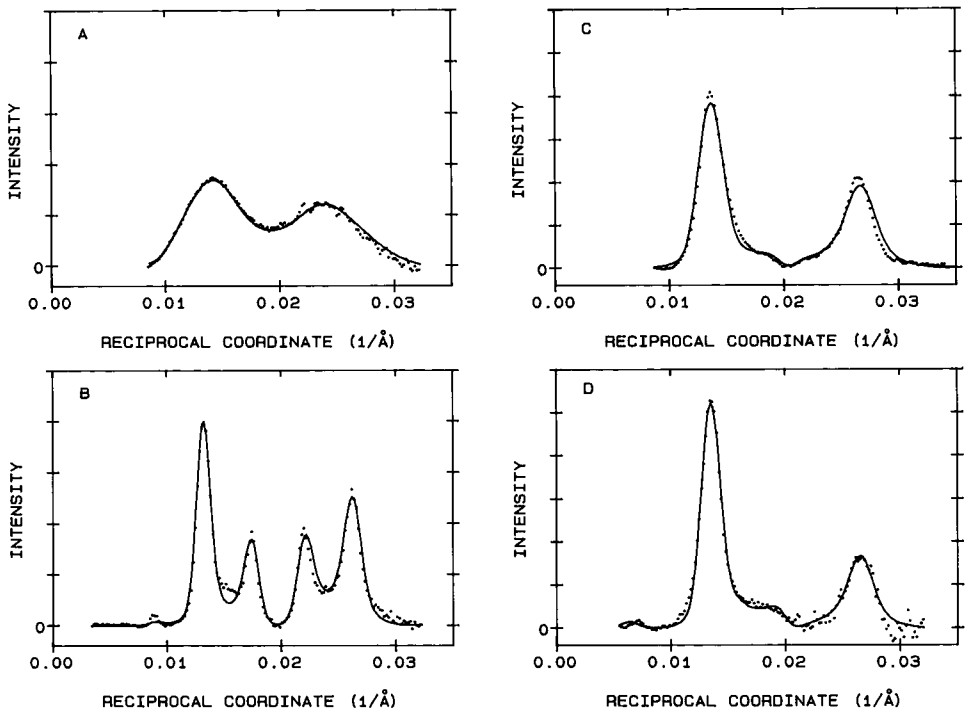

FIGURE 2 Observed (*dotted lines*) and calculated (*solid lines*) intensity distributions from (*A* and *B*) PNS myelin treated at pH 7.4 and ionic strength 0.06, and (*C* and *D*) CNS myelins incubated in distilled water. Panels *A* and *C* are from isolated myelin and *B* and *D* are from similarly treated intact myelin. After background subtraction and Lorentz correction, the curves were normalized.

for by variable vesicle size (Moody, 1975), scattering from unilamellar membranes, scattering from contrast within the membrane surface, or a variation in membrane packing at the cytoplasmic apposition (for example, see model calculation in Fig. 10-8 of Worthington, 1988). Preliminary calculations taking into account vesicle size did not explain the extent of the elevated intensity, and electron micrographs of isolated myelin show neither an abundance of small vesicles nor unilamellar vesicles. The elevated intensity is not observed in diffraction patterns from the well-stacked membranes of intact myelin. However, molecular reorganization that results in the clustering of significant amounts of protein in the membrane surface of isolated myelin cannot be ruled out.

To analyze the variation in cytoplasmic packing of membranes, we used Eq. 8 to calculate the intensity distribution that most closely fit the continuous scattering. The structure factors that were input for the iteration were those for intact myelin treated with normal saline. The period of the "infinitely" swollen myelin was taken to be 500 Å which is a large enough unit cell to adequately sample (in the range 0.01–0.03 $Å^{-1}$) the Fourier transform of a pair of membranes. The initial values for u and β were arbitarily chosen as 40 Å and 10 Å, respectively. The *R*-factor decreased rapidly after several cycles and remained constant at ~10% or better after 2–10 cycles (Fig. 3). The calculated intensity distributions all fit the observed intensities satisfactorily (for example, Fig. 2 *A*). The range in *R*-factors (2–6%) that we found for different diffraction patterns may largely be due to the signal-to-noise of the intensity; smoothing the intensity before

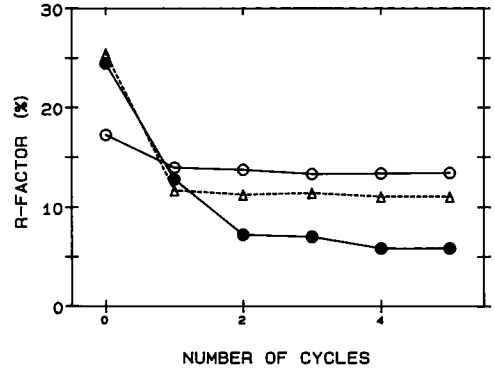

FIGURE 3 Dependence of *R*-factor on the number of least-squares cycles for intact PNS myelin treated at pH 7.4 and ionic strength 0.06 (○), isolated PNS myelin treated at pH 7.4 and ionic strength 0.06 (●), and isolated CNS myelin in distilled water (△).

optimization could reduce this variation and improve the R-factor. Analysis of the continuous scattering to ~30 Å spacing provided optimized structure factors with which we calculated electron density profiles using a one-dimensional Fourier synthesis.

Analysis of diffraction from stacked membranes in isolated myelin

Some diffraction patterns from isolated PNS myelin and all patterns from isolated CNS myelin and intact myelins showed sharp reflections (Fig. 2, *B–D*). The fact that these spacings could be indexed using Bragg's law indicates the membranes are arrayed in lattices; however, the lattices are not perfect. Lattice distortion and the finite extent of the coherence domains of the membrane arrays resulted in an increase in the widths of the reflections with increasing scattering angle (Eq. 7). We estimated initial values for the lattice distortion (Δ), coherence length (N), and myelin periods according to the method described above. Some samples of isolated myelin showed diffuse scattering at ~0.02 $Å^{-1}$ suggesting a variation in the cytoplasmic packing (termed substitution disorder) (Schwartz et al., 1975). The phase of the structure factors changes at about the position of the minimum between the maxima of the continuous intensity distribution (Figs. 1 and 2 *A*). Whenever the diffuse scattering at this position was nearly zero, we assumed that there was no substitution disorder and set β to zero. The initial structure factors were obtained from the integrated intensities of the initially assigned Bragg reflections.

We optimized the structure factors $F(h)$, myelin period d, lattice distortion Δ, cytoplasmic variation β, and coherence length to obtain the closest agreement between the observed and calculated intensity distributions (Eq. 4). Boundary constraints (minimum and maximum values) were imposed on Δ and β. Because the phases of the reflections to 30 Å spacing are agreed upon among researchers, we used these phases as the initial parameters of the structure factors. (All diffraction patterns we examined here were recorded using a point-focus camera. For patterns recorded using a slit-collimated camera, the fit between the calculated and observed intensity was not as satisfactory because the reflections are distorted from a true Gaussian shape.) The R-factors decreased rapidly within several cycles of the least squares optimization (Fig. 3). Generally, the R-factors were smaller in fitting the patterns from isolated myelin than from intact myelin (see Table 1), probably because the sharp reflections from intact myelin are not strictly Gaussian. The optimized structure factors were used in a one-dimensional Fourier synthesis to calculate electron density profiles of the membrane as previously described (Kirschner et al., 1984). The profiles of intact myelin were calculated to a lower resolution to correspond to the limited resolution of the diffraction data from isolated myelin (Karthigasan and Kirschner, 1988).

TABLE 1 Lattice parameters and measurements from electron density profiles for intact and isolated PNS myelin

Sample			d	Δ	u	β	*cyt*	*lpg*	*ext*	N	R
	pH	μ	Å	Å	Å	Å	Å	Å	Å		%
IN		Water	276	9	37	0	30	46	154	8	11
IS		Water	*	*	38	5	32	48	*	1	2
IN	7.4	0.06	228	7	39	0	31	46	105	5	13
IS	7.4	0.06	*	*	38	12	33	46	*	1	6
IN	9.0	0.06	237	11	40	0	33	48	108	6	17
IS	9.0	0.06	*	*	38	12	34	46	*	1	2
IS	7.4	0.15	262	21	38	12	31	46	139	2	15
IN	7.4	0.18	180	4	41	0	35	47	51	‡	19
IS	7.4	0.18	180	7	43	8	35	52	41	2	12
IS	9.0	0.15	179	7	43	10	38	50	41	2	10

IN, intact myelin; IS, isolated myelin; μ, ionic strength; d, myelin period; Δ, lattice distortion; u, packing distance of center of membrane from cytoplasmic apposition; β, standard deviation of $2u$; *cyt*, cytoplasmic space; *lpg*, distance between lipid polar headgroups across the bilayer; *ext*, extracellular space; N, number of periods; R, residual for fit between observed and calculated intensity distribution, rounded to nearest whole percent. *cyt*, *lpg* and *ext* were measured from the calculated electron density profiles.

*Indefinite swelling.

‡The estimate of N becomes inaccurate when the reflection is very sharp and close in width to that of the direct beam (Eq. 7). The accuracy of the parameters is within ±0.5 of their tabulated values.

Electron density profiles of isolated myelin

Profiles for the membranes of isolated myelin resembled membrane profiles of intact myelin and showed a typical bilayer shape, i.e., a pair of electron-dense peaks corresponding to the positions of lipid headgroups were separated by a low-density trough corresponding to lipid hydrocarbon (Fig. 4). The distance between the headgroup peaks and the widths of the spaces between bilayers were measured from these profiles and are compared for isolated and intact myelins in Tables 1 and 2. Also listed are the calculated lattice distortion and variation in width of the membrane separation at the cytoplasmic apposition.

PNS myelin

In hypotonic solution (ionic strength 0.06 or water) the width of the extracellular space of isolated myelin was indefinite, whereas that of intact myelin was finite

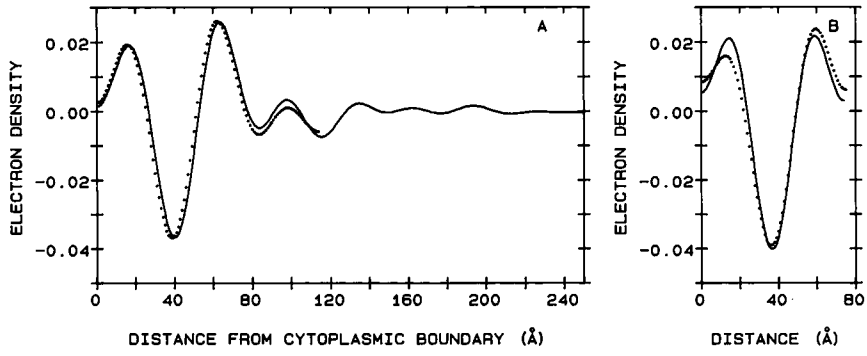

FIGURE 4 Comparison of the electron density profiles (on a relative scale) between intact myelin (*dotted lines*) and isolated myelin (*solid lines*). (*A*) PNS myelins treated at pH 7.4 and ionic strength 0.06. The period of the isolated myelin was arbitrarily chosen as 500 Å. (*B*) CNS myelins incubated in distilled water.

(~100–150 Å) (Fig. 4 *A*; Table 1). In both isolated and intact myelin, the cytoplasmic space was reduced slightly from the native width and the extracellular space was increased; and the electron density level of the headgroup peak at the extracellular side was higher than that at the cytoplasmic side. At the cytoplasmic apposition, the width of the space of isolated myelin was always 1–2 Å greater than that of intact myelin under identical treatment. The variation in the width of the cytoplasmic space β of isolated myelin was 5 Å in distilled water and 12 Å in hypotonic saline at pH 7.4 and pH 9.0, whereas for intact myelin this variation was nearly zero.

In physiological saline (pH 7.4 and ionic strength 0.15) isolated PNS myelin did not show a native period (~180 Å); rather, the period was expanded by nearly 50% due to large swelling at the extracellular apposition. This electron density profile was similar to that of swollen myelin in intact nerve in showing a more electron-dense headgroup peak on the extracellular side. To obtain a native period for isolated myelin required raising the pH to 9.0 or the ionic strength to 0.18 (Karthigasan and Kirschner, 1988). At pH 7.4 and ionic strength 0.18 the profiles of isolated myelin did not fit that of intact myelin perfectly: the isolated myelin showed a 5 Å greater distance between headgroup peaks and a 10 Å narrower extracellular space. The lattice distortion Δ was nearly twofold or more greater for isolated compared with intact myelin. The variation in width of the cytoplasmic space β was appreciable in isolated myelin whereas there was no apparent variation in intact myelin.

TABLE 2 Lattice parameters and measurements from electron density profiles for intact and isolated CNS myelin

Sample		*d*	Δ	*u*	β	*cyt*	*lpg*	*ext*	*N*	*R*
pH	μ	Å	Å	Å	Å	Å	Å	Å		%
IN* 4.1	0.06	153	6	37	0	29	45	34	10	17
IS 4.1	0.06	150	6	38	0	30	45	30	6	11
IS 7.4	0.06	148	7	37	5	29	45	29	4	20
IN* 7.4	0.15	155	6	38	0	32	44	35	23	32
IN* 9.0	0.06	228	11	38	0	29	47	105	4	9
IS 9.0	0.06	153	8	38	11	32	44	33	3	15
IN	Water	150	7	36	0	25	47	31	4	14
IS	Water	148	7	37	0	29	44	31	3	11

See Table 1 for key to symbols. *Data from Inouye and Kirschner, 1989.

CNS myelin

The electron density profiles of isolated CNS myelin appeared to be more symmetric than the intact (e.g., Fig. 4 *B*). This difference is difficult to assess due to the limited resolution of the x-ray data from the isolated myelin. The profiles of isolated myelin at different pH and ionic strength showed similar myelin periods, *cyt*, *lpg*, and *ext* to those of similarly treated intact myelin (Table 2). The dimensions at pH 9 and ionic strength 0.06 were an exception. At pH 4 isolated myelin as well as intact myelin compacted by several angstroms from the 155-Å period of intact myelin at physiological pH and ionic strength. This compaction was due to reduction in the widths of both the cytoplasmic and extracellular spaces. A similar compaction was observed after incubation in distilled water. At pH 7.4 and ionic strength 0.06 isolated myelin showed a single phase of a slightly compacted array (similar to that seen at pH 4 or in distilled water), whereas intact myelin consists of multiple phases (Inouye and Kirschner, 1988*a*). At pH 9.0 and ionic strength 0.06 isolated myelin was slightly compacted whereas intact myelin was greatly swollen at the extracellular apposition. Under any condition the cytoplasmic space in isolated myelin was wider than in intact myelin.

DISCUSSION

Analysis of myelin diffraction patterns

Compared with previous analyses of diffraction from myelin, the procedures that we developed here provide an effective separation of overlapping Bragg peaks, an optimization of the structure factors, and a measure of lattice size and the amount of lattice distortion. The present method utilized the complete optical density data of the diffraction pattern (scaled when necessary from multiple films) and fit the calculated intensity distribution using a nonlinear least squares procedure.

In previous studies of myelin diffraction the structure amplitudes have been determined from the integral area of the Bragg peaks above background (Finean and Burge, 1963; Caspar and Kirschner, 1971; Worthington and McIntosh, 1974). This approach was based on the assumption that the lattice is infinite and not subject to distortion, so that the interference function represented by a δ-function correctly samples the structure amplitude at the Bragg spacings. Whereas this assumption may be appropriate for intact myelin, which gives very sharp reflections to 30 Å spacing or greater, it is less applicable for swollen or isolated myelin which often give broad reflections or continuous scattering. In theory it is possible to determine the structure amplitude from the integral intensity of broad and overlapping reflections when there is no substitution disorder (Worthington and McIntosh, 1974). In practice, however, the separation of overlapping peaks is not trivial and is subject to measurement error. Moreover, such an integration does not allow evaluation of lattice disorder parameters. Higher accuracy is achieved by analyzing the total intensity distribution, as we did here.

Nelander and Blaurock (1978) and Worthington (1986) have calculated the background-corrected intensity distribution for comparison with the observed intensity for PNS myelin, but did not refine all the input parameters. Because the number of sampled points in the observed intensity is greater than that of the number of parameters used to calculate the intensity, a least squares procedure can be utilized. Such a refinement for fitting an entire intensity distribution has been successfully used for the analysis of powder patterns (Young et al., 1980; Wiles and Young, 1981) and for biological membranes (Funk et al., 1981). A least squares procedure has also been applied to the generalized Patterson function (Q-function) of biological membranes including nerve myelin (Pape et al., 1977; Gbordzoe and Kreutz, 1978). In the present work we found that the least squares procedure allowed us to optimize the parameters after relatively few iterations. The initial separation of overlapping peaks may have contributed to the rapid convergence.

Comparing isolated myelin with intact myelin

Coherent domain size

The present x-ray analysis estimated that the number of membrane pairs in the coherent domain for isolated myelin was low: one or two for PNS, and three to six for CNS (Tables 1 and 2). Although this number seems small, electron micrographs of the same specimens used for the x-ray analysis showed that most of the isolated sheaths contained several membrane pairs with only a very small proportion of the sheaths having 10 or more pairs (B. Kosaras, personal communication). A previous estimate from x-ray patterns indicates that the coherent domain for isolated CNS myelin consists of 7–10 bilayers (Sedzik et al., 1984), which corresponds to four or five membrane pairs. The disorder parameters (Δ, β) of intact PNS myelin were similar to those reported previously (Worthington, 1986, 1988).

Cytoplasmic apposition

The cytoplasmic space was often wider and its variation (β) greater in isolated compared with intact myelin for both CNS and PNS; however, in isolated as in intact myelin, the width of this space was nearly invariant as a function of pH and ionic strength. The nature of this apposition has often been thought to be ionic because the positively charged basic protein or putative cytoplasmic domain of P0-glycoprotein and negatively charged phospholipids have been topologically assigned to this surface (Lemke, 1988). The observed invariance in the cytoplasmic separation is not consistent with this notion because ionic interactions should be easily disrupted by changing pH and ionic strength. Myelin is even subjected to hypotonic shock in water during its isolation. Moreover, our calculation of the charge at the cytoplasmic surface shows that its pI is nearly 9 and that the charges of this surface are not neutralized at physiological pH (Inouye and Kirschner, 1988*b*). The involvement of van der Waals or dipole–dipole interactions is consistent with our observation that the cytoplasmic separation is a minimum in distilled water and increases slightly with increasing ionic strength (Blaurock, 1971). It is possible that hydrophobic interactions may also be involved in stabilizing the cytoplasmic apposition.

Extracellular apposition

Maximum compactions of the extracellular space in isolated myelins occurred at pH $\sim$ 4 like that in intact

PNS and CNS myelin (Inouye and Kirschner, 1988*a*). This suggests that the extracellular surfaces of isolated and intact myelins have similar isoelectric points, and that the ionized groups on the extracellular surface are preserved during the isolation procedure.

Unlike the regular swelling that occurs in PNS myelin of intact tissue incubated in distilled water or at low ionic strength (0.06) (Inouye and Kirschner, 1988*a*), an indefinite swelling was observed for isolated PNS myelin. What accounts for this difference in swelling? The present study showed that the electron density profile of the membrane of indefinitely swollen myelin is similar (to a resolution of ~30 Å) to that of the regularly swollen membrane, indicating that a large alteration in molecular organization is unlikely to have caused the difference in swelling response. We have previously determined from a balance of attraction and repulsion forces that the calculated equilibrium periods are larger than the observed periods of intact PNS myelin by ~50 Å at pH 7–9 (see Fig. 3 *C* in Inouye and Kirschner, 1988*b*). If the energy minimum at this equilibrium is very shallow and broad (e.g., Fig. 10 in Inouye and Kirschner, 1988*a*), then the intensity of the x-ray scattering may resemble the continuous scattering from nonarrayed membrane pairs. Another explanation for the indefinite swelling of isolated PNS myelin may be the long-range undulation force that arises from the out-of-plane fluctuations of planar, fluid membranes in multilayer systems (Helfrich, 1978; Evans and Parsegian, 1986). This force, which was ignored in our previous calculations, may be significantly strong in the absence of the mechanical constraints imposed by axon and connective tissue and may result in indeterminate swelling between the membrane pairs.

Distribution of electron density

Isolated PNS myelin like intact myelin shows an increase in the electron density level of the headgroup peak in the extracellular half of the bilayer when the extracellular separation widens in hypotonic media. Although the isolated myelin showed a similar period at neutral pH and ionic strength 0.18, its electron density profile showed an increase (5 Å) of the distance between lipid headgroups and a 10 Å decrease in the width of the extracellular space. Similar changes were found for isolated myelin at pH 9.0 and ionic strength 0.15 when compared with intact myelin (Inouye and Kirschner, 1984). This indicates that the center of mass of some component in isolated myelin shifted toward the extracellular space. The unfolding of the polypeptide chains of P0 glycoprotein on the extracellular surface could account for the shift in mass.

CNS myelin resistance to swelling

Unlike the myelin in intact CNS tissue, the myelin isolated from such tissue does not swell at low ionic strength and alkaline pH (Sedzik et al., 1984; Karthigasan and Kirschner, 1988). This is unexpected in view of evidence suggesting that the extracellular apposition of isolated CNS myelin should swell: cytochemical labeling shows an excess of negative charge at this apposition (Dermietzel et al., 1983); a negative zeta-potential is measured for vesicles of CNS myelin (Moscarello et al., 1985); and modeling of the membrane surfaces and their charge based on biochemical data indicates a net negative charge at pH > 4 (Inouye and Kirschner, 1988*b*). As discussed previously (Karthigasan and Kirschner, 1988), the resistance to swelling could be due to a structural reorganization of proteolipid protein, the binding of divalent cations, or enrichment in interlamellar tight junctions during isolation. The electron density profiles calculated in the current paper did not show, to a resolution of 30 Å, any major structural rearrangement. While interlamellar tight junctions have recently been observed in isolated myelin (B. Kosaras, personal communication), it is not certain whether these specialized structures are actually enriched in the membranes. Therefore, the resistance of isolated CNS myelin to swelling has yet to be determined.

CONCLUSIONS

Analysis of x-ray diffraction patterns from myelin membranes that have been isolated fron intact tissue has been hampered by the presence of broad Bragg reflections or continuous scattering. We have now developed nonlinear least squares procedures for interpreting such patterns, and have calculated for the first time electron density profiles of isolated myelin membranes for comparison with those of intact myelin. Our results show that at least to a resolution of ~30 Å there is close correspondence between the membrane bilayer profiles for isolated and intact myelins, even when there is a difference in the width of the extracellular space between membranes. Efforts directed toward obtaining higher resolution diffraction patterns from isolated myelin can be anticipated. This study together with our earlier one (Karthigasan and Kirschner, 1988) provide an approach for the investigation of membrane structure and interactions in the myelin isolated from the pathological tissue of multiple sclerosis and other demyelinating diseases.

We thank Dr. Bela Kosaras for valuable discussions about the structure of isolated myelin.

This research was supported by National Institutes of Health grant NS-20824 (D. A. Kirschner) from the National Institute of Neurological and Communicative Disorders and Stroke. The work was carried out in facilities of the Mental Retardation Research Center which is supported in part by National Institutes of Health Center Grant

P30-HD 18655 for the National Institute of Child Health and Human Development.

Received for publication 7 November 1988 and in final form 27 March 1989.

REFERENCES

Alexander, L. E. 1969. X-Ray Diffraction Methods in Polymer Science. John Wiley & Sons, New York. 423 pp.

Bevington, P. R. 1969. Data reduction and error analysis for the physical sciences. McGraw-Hill Book Co., New York. 235–237.

Blaurock, A. E. 1971. Structure of the nerve myelin membrane: proof of the low resolution profile. *J. Mol. Biol.* 56:35–52.

Caspar, D. L. D., and D. A. Kirschner. 1971. Myelin membrane structure at 10 Å resolution. *Nature (Lond.)* 231:46–52.

Dermietzel, R., N. Thurauf, and D. Schunke. 1983. Cytochemical demonstration of negative surface charges in central myelin. *Brain Res.* 262:225–232.

Evans, E. A., and V. A. Parsegian. 1986. Thermal-mechanical fluctuations enhance repulsion between bimolecular layers. *Proc. Natl. Acad. Sci. USA.* 83:7132–7136.

Finean, J. B., and R. E. Burge. 1963. The determination of the Fourier transform of the myelin layer from a study of swelling phenomena. *J. Mol. Biol.* 7:672–682.

Funk, J., W. Welte, N. Hodapp, I. Wutschel, and W. Kreutz. 1981. Evaluation of the electron density profile of the frog rod outer segment disc-membrane in vivo using x-ray diffraction. *Biochim. Biophys. Acta.* 640:142–158.

Gbordzoe, M. K., and W. Kreutz. 1978. Direct x-ray determination of the electron density profile of the nerve myelin membrane, with paracrystalline lattice distortions taken into account. *J. Appl. Crystallogr.* 11:489–495.

Guinier, A. 1963. X-ray Diffraction. P. Lorrain and D. S.-M. Lorrain, translators. W. H. Freeman and Co., San Francisco, CA.

Helfrich, W. 1978. Steric interaction of fluid membranes in multilayer systems. *Z. Naturforsch.* 33a:305–315.

Hosemann, R., and S. N. Bagchi. 1962. Direct Analysis of Diffraction by Matter. Elsevier/North Holland, Amsterdam.

Inouye, H., and D. A. Kirschner. 1984. Effects of $ZnCl_2$ on membrane interactions in myelin of normal and shiverer mice. *Biochim. Biophys. Acta.* 776:197–208.

Inouye, H., and D. A. Kirschner. 1988*a*. Membrane interactions in nerve myelin. I. Determination of surface charge from effects of pH and ionic strength on period. *Biophys. J.* 53:235–246.

Inouye, H., and D. A. Kirschner. 1988*b*. Membrane interactions in nerve myelin. II. Determination of surface charge from biochemical data. *Biophys. J.* 53:247–260.

Inouye, H., and D. A. Kirschner. 1989. Orientation of proteolipid protein in myelin: comparison of models with x-ray diffraction measurements. *Dev. Neurosci.* In press.

Karthigasan, J., and D. A. Kirschner. 1988. Membrane interactions are altered in myelin isolated from central and peripheral nervous system tissues. *J. Neurochem.* 51:228–236.

Kirschner, D. A., and D. L. D. Caspar. 1972. Comparative diffraction studies on myelin membrane. *Ann. N. Y. Acad. Sci.* 195:309–320.

Kirschner, D. A., A. L. Ganser, and D. L. D. Caspar. 1984. Diffraction studies of molecular organization and membrane interactions in myelin. *In* Myelin. P. Morell, editor. Plenum Publishing Corp., New York. 51–95.

Lemke, G. 1988. Unwrapping the genes of myelin. *Neuron.* 1:535–543.

Moody, M. F. 1975. Diffraction by dispersions of spherical membrane vesicles. I. The basic equations. *Acta Crystallogr.* A31:8–15.

Moscarello, M. A., L.-S. Chia, D. Leighton, and D. Absolom. 1985. Size and surface charge properties of myelin vesicles from normal and diseased (multiple sclerosis) brain. *J. Neurochem.* 45:415–421.

Nelander, J. C., and A. E. Blaurock. 1978. Disorder in nerve myelin: phasing the higher order reflections by means of the diffuse scatter. *J. Mol. Biol.* 118:497–532.

Norton, W. T., and S. E. Poduslo. 1973. Myelination in rat brain: method of myelin isolation. *J. Neurochem.* 21:749–757.

Pape, E. H., K. Klott, and W. Kreutz. 1977. The determination of the electron density profile of the human erythrocyte ghost membrane by small-angle x-ray diffraction. *Biophys. J.* 19:141–161.

Schwartz, S., J. E. Cain, E. A. Dratz, and J. K. Blasie. 1975. An analysis of lamellar x-ray diffraction from disordered membrane multilayers with application to data from retinal rod outer segments. *Biophys. J.* 15:1201–1233.

Sedzik, J., A. D. Toews, A. E. Blaurock, and P. Morell. 1984. Resistance to disruption of multilamellar fragments of central nervous system myelin. *J. Neurochem.* 43:1415–1420.

Toraya, H., M. Yoshimura, S. Sōmiya. 1983. A computer program for the deconvolution of x-ray diffraction profiles with the composite of Pearson type VII functions. *J. Appl. Crystallogr.* 16:653–657.

Wiles, D. B., and R. A. Young. 1981. A new computer program for Rietveld analysis of x-ray powder diffraction patterns. *J. Appl. Crystallogr.* 14:149–151.

Worthington, C. R. 1986. Diffuse scattering problem in membrane diffraction: a solution. *Biophys. J.* 49:98–101.

Worthington, C. R. 1988. X-ray diffraction and the membrane states of nerve myelin. *In* Advances in Membrane Fluidity. Vol. 1. R. C. Aloya, C. C. Curtain, and L. M. Gordon, Alan R. Liss, Inc., New York. 239–266.

Worthington, C. R., and A. E. Blaurock. 1969. A structural analysis of nerve myelin. *Biophys. J.* 9:970–990.

Worthington, C. R., and T. J. McIntosh. 1974. Direct determination of the lamellar structure of peripheral nerve myelin at moderate resolution (7 Å). *Biophys. J.* 14:703–729.

Young, R. A., J. L. Lundberg, and A. Immirzi. 1980. Application of the Rietveld whole-fitting method in linear polymer structure analysis. *In* Fiber Diffraction Methods. A. D. French and K. C. Gardner, editors. American Chemical Society Symposium Series Washington, DC. 141:69–91.